Dynamical diagnostics for the glass transition in soft-sphere alloys

1989 J. Phys.: Condens. Matter 1 7171

(http://iopscience.iop.org/0953-8984/1/39/028)

J. Phys.: Condens. Matter 1 (1989) 7171–7186. Printed in the UK

Dynamical diagnostics for the glass transition in soft-sphere alloys

J N Roux, J L Barrat and J-P Hansen
Laboratoire de Physique, Unité de Recherche Associée 1325 du CNRS, Ecole Normale Supérieure de Lyon, 69364 Lyon Cedex 07, France

Received 10 April 1989

Abstract. The structural slowing down in a binary alloy of soft spheres near the fluid–glass transition has been investigated by extensive molecular dynamics simulations. An attempt is made to characterise the transition on the basis of *r*- and *k*-space representations of the incoherent and coherent parts of the density autocorrelation functions. A careful analysis of the Van Hove functions allows us to put forward two novel diagnostics of the underlying 'ideal' glass transition, which yield the same value of the critical glass transition temperature. The latter appears to be independent of the mass ratio of the two species in the mixture. The damping of the longitudinal sound mode at the longest accessible wavelength appears to be surprisingly independent of temperature, while the damping of the corresponding transverse sound mode decreases significantly as the temperature is lowered.

1. Introduction

Several recent inelastic neutron scattering measurements of the density fluctuation spectrum in supercooled ionic [1, 2] or polymeric [3, 4] liquids show evidence of the critical behaviour predicted by mode-coupling theories of the dynamical liquid–glass transition [5–13]. The sharp transition from ergodic to non-ergodic behaviour of the density autocorrelation function ('structural arrest') predicted by the simplest version of mode-coupling theory (the so-called 'ideal' glass transition) [5, 6] has also been observed in molecular dynamics (MD) simulations of a supercooled Lennard-Jones liquid [14]. The obvious diagnostics signalling such an 'ideal' glass transition are the discontinuous appearance of strictly non-decaying Fourier components of the density autocorrelation function and the vanishing of the self-diffusion constant. However the 'ideal' glass transition is smeared by activated processes, which lead to residual diffusion of atoms in the glassy state and restore ergodicity on a sufficiently long timescale. This behaviour may be accounted for by an improved version of the original mode-coupling theory, which allows for coupling to current fluctuations [12, 13]. Evidence for the importance of activated processes is contained in recent MD simulations of simple binary soft-sphere alloys [15, 16].

Discarding the latter processes, the most striking prediction of the mode-coupling analysis is the existence of two clearly distinct regimes of low-frequency dynamics, which may be associated with α (or primary) and β (or secondary) relaxation, and are characterised by scaling laws with non-universal exponents. The two dynamic regimes

0953-8984/89/397171 + 16 $02.50

and their scaling behaviour are clearly evident in the spectra of the density correlation function of the ionic glass former $Ca_{0.4}K_{0.6}(NO_3)_{1.4}$ measured by a combination of spin echo and time-of-flight neutron scattering experiments, which cover a time interval of over four decades (from 10^{-13} to over 10^{-9} s) [1, 2]. While MD simulations carried out on simple model systems typically cover comparable time spans, the insufficient sampling of phase space, associated with the dramatic slowing down of structural rearrangements, leads to poor statistics on the computed coherent and incoherent density autocorrelation functions. Consequently it appears *a priori* difficult to extract quantitative information on the subtle dynamical behaviour near the glass transition from MD simulations. However, MD has the advantage of yielding information on a variety of correlation functions, which are not accessible to radiation scattering techniques. In particular, coherent and incoherent density fluctuations are readily separated, and real-space correlation functions are as easily computed as their k-space counterparts.

In this paper we take advantage of this flexibility to explore density correlations in real space (i.e. the Van Hove functions) together with their spatial Fourier transforms (the so-called intermediate scattering functions) in an attempt to develop alternative diagnostics of the ideal glass transition and of the influence of activated processes. In the second part of the paper we examine the propagation of long-wavelength longitudinal and transverse sound modes in the vicinity of the glass transition. The main problem at issue here is how the damping of sound waves evolves as the temperature is lowered from the liquid into the glass phase, which is characterised by extremely large values of the viscosity. All simulations were carried out on a simple binary soft-sphere model to be defined in the next section.

2. Model and numerical procedures

The binary model alloy that has been simulated is identical to that used in some earlier MD work [15–19]. The binary soft-sphere mixture contains N_1 atoms of mass m_1 and diameter σ_1 and N_2 atoms of mass m_2 and diameter σ_2 in a volume V. These interact via the purely repulsive inverse-12 pair potentials:

$$V_{\alpha\beta}(r) = \varepsilon(\sigma_{\alpha\beta}/r)^{12} \tag{1}$$

where $1 \leqslant \alpha, \beta \leqslant 2$ are species indices and the diameters are taken to be additive, i.e. $\sigma_{\alpha\beta} = (\sigma_\alpha + \sigma_\beta)/2$. The advantages of considering this model for an investigation of the glass transition have been discussed at length elsewhere [17]. Briefly speaking, nucleation of a crystal is easily bypassed in binary systems, whereas the behaviour of the corresponding one-component system is very sensitive to the quenching rate [20]. Crystallisation of an undercooled binary liquid would require a phase separation of the two species, which are not miscible in the crystalline solid above some critical ratio of the diameters ($\sigma_2/\sigma_1 \geqslant 1.15$) [21]. The corresponding inter-diffusion process is extremely slow near the glass transition, thus preventing the formation of the inhomogeneity required in the nucleation process. Thus the very long runs required for a study of the slowing down of structural relaxation can be carried out safely, whereas the supercooled one-component fluid always exhibits a tendency towards spontaneous nucleation over sufficiently long time intervals.

On the other hand the choice of a soft-sphere mixture, rather than a more 'realistic' model like e.g. a binary Lennard-Jones mixture [22], is dictated by three different considerations. First, the scaling properties of inverse-power potentials imply a

reduction of the independent thermodynamic variables for the mixture from three to two. Secondly, the properties of the one-component version of the model are well documented [23–25]. Thirdly, the absence of attractive forces between atoms allows one to focus on steric (excluded-volume) effects near the glass transition.

Let $x_\alpha = N_\alpha/N$ (with $N = N_1 + N_2$) denote the number concentrations of the two species ($x_1 + x_2 = 1$). According to conformal solution theory, the concentration-dependent diameter of an 'effective' one-component system would be [17]

$$\sigma_x^3 = x_1^2\sigma_1^3 + 2x_1x_2\sigma_{12}^3 + x_2^2\sigma_2^3. \tag{2}$$

A convenient choice of independent state variables is then the pair consisting of x_1 and the effective coupling constant

$$\Gamma = \rho_x^* (T^*)^{-1/4} \tag{3}$$

where $\rho_x^* = N\sigma_x^3/V$ denotes the effective reduced density and $T^* = k_B T/\varepsilon$ denotes the reduced temperature. Note that for fixed x_1, a given value of the coupling constant Γ can be achieved either by cooling the mixture at constant density or by compressing it at constant temperature. As long as the system remains in thermodynamic equilibrium, the final state (x_1, Γ) is independent of the route followed, but this is not necessarily true when the final state corresponds to a metastable glassy state. It may be noted at this stage that, within the mode-coupling theories [5–13], the quantities that characterise the glass transition depend only on the usual thermodynamic variables of equilibrium states.

The microscopic timescale is measured in units of $\tau = (m_1\sigma_1^2/\varepsilon)^{1/2}$, which turns out to be of the order of the inverse of the Einstein frequencies $\Omega_{E\alpha}$ associated with the two species [17]. The simulations reported in this paper were carried out for a size ratio $\sigma_2/\sigma_1 = 1.2$, which is more 'realistic' than the larger ratio of 1.4 used in some earlier work [15–17] if metallic alloys are to be modelled. Most calculations were carried out for a mass ratio $m_2/m_1 = 2$, but some exploratory runs were made with $m_2/m_1 = 10$, to check the influence of the mass ratio on the glass transition. The latter would of course be independent of the mass ratio within classical statistical mechanics, if it were a genuine equilibrium thermodynamic phase transition. All results reported here are for equimolar mixtures ($x_1 = x_2 = \frac{1}{2}$).

Based on earlier simulations for the one-component version of the model [23], and for mixtures with the same [18] or different [15–17] size ratios, we expect the glass transition to take place around $\Gamma \simeq 1.5$. The one-component soft-sphere fluid freezes at $\Gamma \simeq 1.15$ [24, 25], but by analogy with the phase diagram of binary hard-sphere mixtures with a similar ratio σ_2/σ_1, the present soft-sphere fluid–solid coexistence curve should exhibit a eutectic at a higher value of Γ, for a relatively low concentration of the larger species ($x_2 \simeq 0.1$).

We have systematically explored the supercooled fluid phase of the equimolar mixture over the coupling range $1.3 \leqslant \Gamma \leqslant 1.5$, by constant-temperature MD simulations of samples of $N = 432$ atoms in a dodecahedral cell with periodic boundary conditions, using the standard Verlet algorithm [26] with a time step of typically $\Delta t^* = \Delta t/\tau = 0.012$. In contrast to much of the earlier work, the sample was generally quenched by gradual compression, rather than by rapid cooling. A few test runs using the latter procedure showed no significant differences in the behaviour of the quenched samples for identical final values of Γ. The successive states of two independent quenching histories are summarised in table 1. Two successive compressions were typically separated by 10^5 time steps for equilibration, and averages were taken over at least 5×10^4 time steps. If the potential parameters ε and σ_1 are given values typical e.g. of argon, the resulting

Table 1. Two cooling histories near the glass transition. T_{eq} = time for equilibration after the initial compression (in units of τ). T_m = time during which the system is followed in phase space after equilibration (in units of τ). Each initial configuration is obtained on rescaling the particle coordinates of the last configuration of the preceding run in the list, unless otherwise stated.

Run No	Γ	T_{eq}	T_m
a1	1.42	500	500
a2	1.44	600	600
a3	1.46	600	600
a4	1.48	1200	600
a5	1.50	1440	600
b1	1.42	120	360 (from a1)
b2	1.43	600	600
b3	1.44	600	120
b4	1.45	1200	600
b5	1.455	1800	600

equivalent cooling rate would be of the order of 10^9 K s^{-1}, which is comparable to those achieved by the fastest experimental techniques, and considerably less than the ultra-high cooling rates generally reported for 'computer glass'. Positions and velocities of all particles were recorded on discs every five time steps to allow subsequent computation of static and time-dependent correlation functions, which serve as diagnostics for the glass transition.

3. Static diagnostics

The three partial pair distribution functions $g_{\alpha\beta}(r)$ and the corresponding static structure factors $S_{\alpha\beta}(k)$ are readily calculated by averaging over MD-generated configurations. They behave very much as already observed for the same model with the larger ratio $\sigma_2/\sigma_1 = 1.4$ [17]. In particular they vary quite smoothly over the range of Γ-values investigated, they are perfectly reproducible, i.e. do not depend on the quench history, and they are independent of the mass ratio m_2/m_1; the latter ergodicity property is rigorously true only for equilibrium states, but our MD results suggest that it remains well verified for quenched (metastable) states. The $g_{\alpha\beta}(r)$ allow a direct calculation of the first derivatives of the free energy, i.e. the pressure P and the internal energy U. Since derivatives with respect to density and temperature are equivalent in the present soft-sphere model, the excess pressure and internal energy are directly proportional to each other. As already observed for the corresponding one-component system [23], and for the mixture with $\sigma_2/\sigma_1 = 1.4$ [17], the dimensionless equation of state

$$Z = PV/Nk_BT$$

is, to an excellent approximation, a linear function of Γ^4 (i.e. of $1/T$ for a fixed density). As in [17], we have also determined the pair structure and Z from a thermodynamically self-consistent integral equation due to Rogers and Young (RY) [27], which is known to be very accurate for inverse-power potentials. The MD and RY results for the equation of state agree within the error bars of the former data, up to $\Gamma \simeq 1.45$, but for larger

couplings (i.e. lower temperatures) the RY data drop significantly below the MD results [19]. This 'bifurcation' was interpreted in [17] as a first indication of the glass transition, under the assumption that the integral equation describes the fully relaxed supercooled liquid state, while the MD data correspond to quenched glassy states that do not have time to relax to the lowest free energy state over the observation time interval, which remains very short in view of the rapidly increasing structural relaxation time. This view is consistent with the fact that the free energy, calculated by integrating the equation of state, is lower for the RY than for the MD results.

The isothermal bulk modulus (or inverse compressibility) B_T can be calculated from a numerical differentiation of the equation of state or directly from the appropriate combination of the isothermal elastic constants ($B_T = (C_{11} + 2C_{12} + P)/3$), which are given by standard fluctuation formulae involving pair, three- and four-point correlation functions [19]. The MD data, which are affected by about 5% error bars, vary smoothly with Γ and bifurcate from the corresponding integral-equation results around $\Gamma \simeq 1.45$ [19]. The MD data show no sign of any discontinuity or rapid variation in the vicinity of this smooth bifurcation. The same is hence true of the constant-volume specific heat, C_v, which is directly related to the bulk modulus in the present soft-sphere model. Similarly C_p, which is related to C_v by a standard thermodynamic formula, appears to vary smoothly across the transition. This behaviour, which contrasts with the rounded specific heat jumps observed for many laboratory glass formers, is probably characteristic of the soft-sphere model where atoms interact only with their closest neighbours due to the short range of the pair potential. In particular, the absence of an attractive tail prevents the potential from probing the subtle structural rearrangements occurring on intermediate distance scales.

We have finally computed the shear modulus

$$G = C_{44} - P = (C_{11} - C_{12} - 2P)/2$$

in an isotropic solid like a glass. The MD results have been presented in a preliminary note [19]; they show that G vanishes, within statistical errors, around $\Gamma \simeq 1.45$. In the glass ($\Gamma \geqslant 1.45$) G turns out to be significantly smaller than in a polycrystalline sample under the same density–temperature conditions.

It should be stressed that the 'static' quantities computed here are characteristic of the glassy states for frequencies of the order of the inverse observation time (typically 10^9 Hz). For much lower frequencies (i.e. for macroscopic observation times), these properties may gradually change and tend towards their metastable 'liquid' values. In particular, for very long observation times, G may decrease towards zero, even for $\Gamma \geqslant 1.45$, since the response of the supercooled mixture is expected to cross over from elastic to viscous (with very large values of the shear viscosity η).

4. Single-particle motion

In its simplest version, in which the memory kernel includes the non-linear feedback from density fluctuations only, mode-coupling theory predicts that the self-diffusion constants vanish according to a critical power law, at the temperature T_0 of the 'ideal' glass transition. This power law is compatible with the results of earlier MD simulations of binary soft-sphere mixtures, with a 'critical exponent' that turns out to be the same for both species, and has a value close to 2 [17]. However, these same MD simulations clearly show that, in the immediate vicinity of T_0, jump diffusion, related to activated

processes, takes over, so that D_1 and D_2 deviate more and more from a power law and do not vanish at the glass transition. Jump diffusion processes have been investigated in more detail [16], but since they are very rare events, the resulting diffusion constants D_1 and D_2 are very small (typically two orders of magnitude smaller than in the stable liquid near the freezing point) and not reproducible in different runs, in the immediate vicinity of the glass transition.

The present simulations, carried out for the size ratio $\sigma_2/\sigma_1 = 1.2$, very much confirm the above observations. For $\Gamma \geqslant 1.44$, the slope of the mean-square displacement of atoms of one species $\langle|\boldsymbol{r}^{(\alpha)}(t) - \boldsymbol{r}^{(\alpha)}(0)|^2\rangle$ changes with time t, so that the resulting apparent diffusion constant D_α ($\alpha = 1, 2$) is not well defined; the uncertainty is typically as large as a factor of 2. Reliable and reproducible results for the D_α (with statistical errors of 10% or less) are observed only at higher temperatures in the supercooled liquid range (typically for $\Gamma \leqslant 1.42$). These results fall on two parallel straight lines in a plot of $\ln D_\alpha^*$ versus $\ln(\Gamma_0 - \Gamma)$, where

$$D_\alpha^* = D_\alpha \tau \sigma_1^2 (T^*)^{-5/12}$$

is the reduced diffusion constant of species α, which depends only on the state variables Γ and x_1 [17]; the best straight-line fits are obtained for $\Gamma_0 \simeq 1.5$ and a slope (i.e. a critical exponent) $\nu \simeq 2$.

In order to obtain a clearer and more quantitative picture of the space and time dependences of single-particle motion we have computed the self-parts of the density autocorrelation (or Van Hove) functions, namely

$$G_s^{(\alpha)}(\boldsymbol{r}, t) = (1/N_\alpha) \sum_{i=1}^{N_\alpha} \langle \delta(\boldsymbol{r}_i(t) - \boldsymbol{r}_i(0) - \boldsymbol{r}) \rangle \tag{4}$$

where $\boldsymbol{r}_i^{(\alpha)}(t)$ denotes the position of particle i of species α at time t. In the stable or moderately supercooled liquid, the $G_s^{(\alpha)}$ are expected to go over rapidly to their hydrodynamic limit for $t \gg \tau$, i.e.

$$G_s^{(\alpha)}(\boldsymbol{r}, t) \simeq \frac{1}{(4\pi D_\alpha t)^{3/2}} \exp\left(\frac{-r^2}{4D_\alpha t}\right). \tag{5}$$

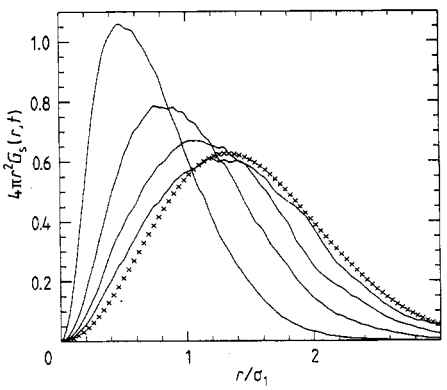

Figure 1. $r^2 G_s^1(r, t)$ versus $x = r/\sigma_1$ at $\Gamma = 1.42$ (and $m_2/m_1 = 2$). The full curves from left to right correspond to times $t^* = t/\tau = 50$, 100, 150 and 200. The crosses represent the hydrodynamic result (5) for $t^* = 200$, calculated with the measured value of D_1.

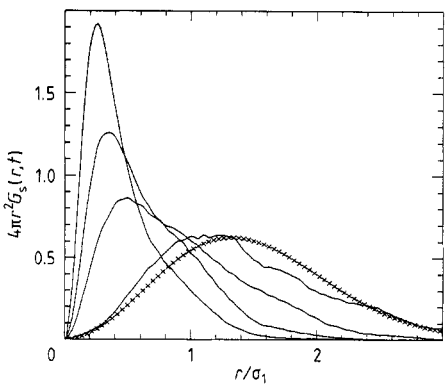

Figure 2. Same as in figure 1, but for $\Gamma = 1.45$ and $t^* = 46$, 92, 229 and 458.

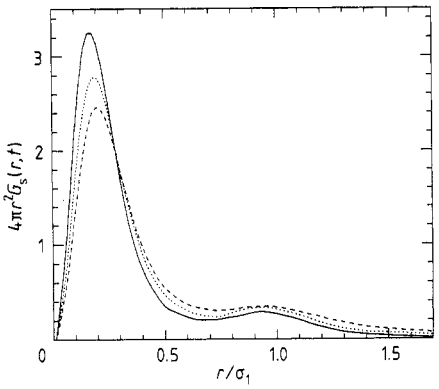

Figure 3. Same as in figure 1, but for $\Gamma = 1.46$ and $t^* = 108$ (full curve), 216 (dotted curve) and 324 (broken curve).

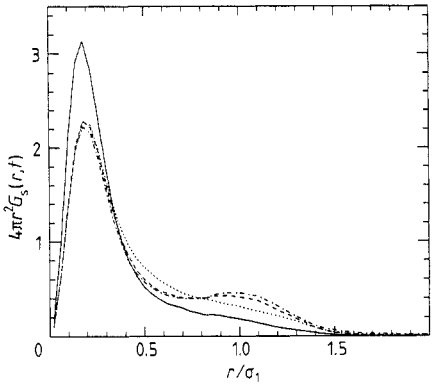

Figure 4. Same as in figure 1, but for $\Gamma = 1.48$ and $t^* = 120$ (full curve), 240 (dotted curve), 360 (broken curve) and 480 (chain curve).

The mean-square displacement of an atom after a time t is equal to the second moment of $G_s^{(\alpha)}(\boldsymbol{r}, t)$, i.e.

$$\langle |\boldsymbol{r}_i^{(\alpha)}(t) - \boldsymbol{r}_i^{(\alpha)}(0)|^2 \rangle = \int r^2 G_s^{(\alpha)}(\boldsymbol{r}, t)\, \mathrm{d}^3 r. \tag{6}$$

The integrand $r^2 G_s^{(\alpha)}(r, t)$ has a maximum (at $r_m^{(\alpha)} = 4D_\alpha t$ in the hydrodynamic limit (5)) that moves more and more slowly to larger r as the diffusion constant drops with increasing Γ. In a completely frozen structure (i.e. in a low-temperature crystal or glass), the maximum of $r^2 G_s(r, t)$ stabilises, after a time of the order of the inverse Einstein frequency $\tau_E = 1/\Omega_E$, at a fixed value determined by the Debye–Waller factor, i.e. $r_m^{(\alpha)} = 2\langle u_\alpha^2 \rangle$, where u_α denotes the thermal deviation of an atom of species α from its equilibrium position.

We have investigated the behaviour of $G_s^{(\alpha)}(r, t)$ in the supercooled liquid, as the glass transition is approached. Representative MD results for $r^2 G_s^{(1)}(r, t)$ at different couplings are shown in figures 1–4. In each figure $r^2 G_s^{(1)}(r, t)$ is plotted versus r for three or four different time arguments. At the highest temperature ($\Gamma = 1.42$), the peak in $r^2 G_s^{(1)}(r, t)$ is seen to move reasonably fast to larger r and the hydrodynamic limit (5) is reproduced rather accurately after $t^* = t/\tau \simeq 200$. Deeper in the supercooled liquid ($\Gamma = 1.45$), the behaviour is qualitatively still the same, although the single-particle motion has by now slowed down significantly, and the hydrodynamic limit is not yet fully reached after the longest time accessible in the simulation (here $t/\tau \simeq 450$). An unmistakable qualitative change appears, however, at the slightly stronger coupling $\Gamma = 1.46$ (cf figure 3). The position of the main peak in $r^2 G_s(r, t)$ is now independent of time, even for the longest times investigated, while its amplitude and its area decrease gradually with time. Since $G_s^{(\alpha)}(r, t)$ is normalised to unity at all times, the 'missing intensity' reappears as a tail at larger r, which extends to distances of the order of the mean inter-atomic spacing; the 'intensity' of this tail gradually increases with time, thus compensating the losses under the first peak. These features are reproducible, although the detailed shape of the tail at large r differs somewhat from run to run. The behaviour at the slightly stronger coupling ($\Gamma = 1.48$) is very similar (cf. figure 4).

The physical interpretation of the qualitative changes in $G_s^{(\alpha)}(r, t)$ is quite transparent. For $\Gamma < 1.46$, diffusion is not unlike that observed in liquids, except for a gradual

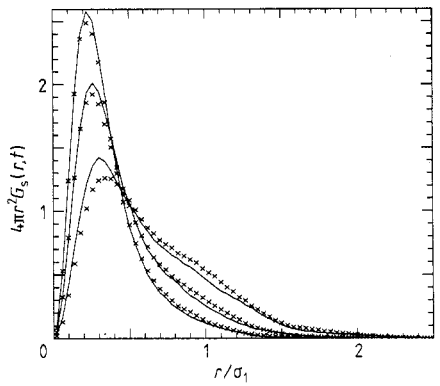

Figure 5. A test of time scaling; $r^2 G_s^1(r, t)$ is plotted versus r/σ_1 at $\Gamma = 1.43$ (full curve) and $\Gamma = 1.45$ (crosses) for $t^* = n\tau_\Gamma^*$ $(n = 1, 2, 3)$, where the time intervals $\tau_\Gamma^* = 16.3$ (for $\Gamma = 1.43$) and 23 (for $\Gamma = 1.45$) are taken in the ratio of the measured self-diffusion coefficients $D_1(\Gamma)$.

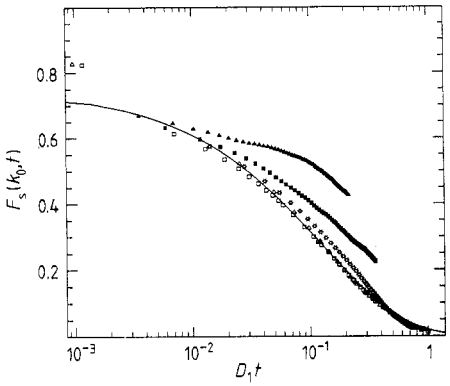

Figure 6. The self-intermediate scattering function $F_s^1(k, t)$ plotted versus $\ln(D_1^* t^*)$ for $k = k_0$ (position of the main peak in the number structure factor $S_{nn}(k)$). Open squares, $\Gamma = 1.4$; open triangles, $\Gamma = 1.42$; stars, $\Gamma = 1.44$; full squares, $\Gamma = 1.46$; full triangles, $\Gamma = 1.48$. The full curve is a Kohlrausch 'master curve' $A \exp(-s^\beta)$ fitted to the data at the three lower Γ values; the fit yields $A = 0.75$ and $\beta = 0.62$.

slowing down; the hydrodynamic diffusion limit (5) is reached only after increasingly long time intervals. All atoms diffuse and single-particle motion is intimately related to the gradual break-up of the local structure, as will become apparent in the following section. A comparison between the results for $\Gamma = 1.43$ and $\Gamma = 1.45$ displayed in figure 5 shows that $G_s^{(\alpha)}(r, t)$ approximately scales with $D_\alpha t/\sigma_1^2$, well before the hydrodynamic limit (5) is reached (where this scaling property is of course exact). For $\Gamma \geqslant 1.46$ the main peak in $r^2 G_s^{(\alpha)}(r, t)$ appears at a position that is independent of time, even for the longest time intervals explored in our MD runs; this points to a frozen, disordered structure where most atoms vibrate around fixed equilibrium positions. The quenched disordered structure exhibits many defects (vacancies, interstitials) compared to a regular crystalline stucture, and relaxes very slowly (on a timescale much longer than the 10^{-9} s typically explored by MD runs) via activated processes, like individual or correlated jumps [16]. These rare processes give rise to the large-r tail in $r^2 G_s^{(\alpha)}(r, t)$, which builds up very gradually, at the expense of the area under the frozen main peak. The position of the latter allows an unambiguous determination of the 'Lindemann ratio' $L_\alpha = (\langle u_\alpha^2 \rangle / d^2)^{1/2}$, where d denotes the mean inter-particle spacing [6], as determined e.g. from the position of the first peak in the total pair distribution function. A few typical MD results are listed in table 2. At the glass transition ($\Gamma \simeq 1.46$), the Lindemann ratios are comparable to their values in a crystalline solid near melting.

The incoherent part of the inelastic neutron scattering cross section is directly related to the self-intermediate scattering functions $F_s^{(\alpha)}(k, t)$, which are the spatial Fourier transforms of the $G_s^{(\alpha)}(r, t)$:

$$F_s^{(\alpha)}(k, t) = (1/N_\alpha) \sum_{i=1}^{N_\alpha} \langle \exp\{i\boldsymbol{k} \cdot [\boldsymbol{r}_i^{(\alpha)}(t) - \boldsymbol{r}_i^{(\alpha)}(0)]\} \rangle. \tag{7}$$

The signature of an 'ideal' glass transition, where activated processes are neglected, is the discontinuous change in behaviour of $F_s^{(\alpha)}(k, t)$ from ergodic before the transition

Table 2. Measured values of Lindemann ratios. $L^{(\alpha)} = \langle u_\alpha^2 \rangle^{1/2}/d$ for species α, where u_α is the displacement of a particle from its equilibrium position and d is the average distance between two nearest neighbours. We have conventionally chosen for d the position of the first peak of $g_{nn}(r)$, the *total* density autocorrelation function. With this definition, $L^{(1)}$ and $L^{(2)}$ appear to be equal within the accuracy of the measurements.

	Γ	$L^{(1)} \simeq L^{(2)}$
Glass	1.46	0.19
Glass	1.48	0.17
Glass	1.50	0.15
CsCl crystal	1.46	0.14

($\Gamma < \Gamma_0$) to non-ergodic in the glass ($\Gamma > \Gamma_0$) ('structural arrest'); in the latter case $F_s^{(\alpha)}(k, t)$ tends to a k-dependent non-zero limit (the so-called Edwards–Anderson order parameters [28]) as $t \to \infty$. Such a behaviour has indeed been confirmed by neutron scattering experiments [1, 2] and by MD simulations [14, 15], at least in the time windows explored by these probes of microscopic dynamics. However, activated processes will restore ergodicity after much longer times, so that $F_s^{(\alpha)}(k, t)$ is expected to decay ultimately to zero, even for $\Gamma > \Gamma_0$.

MD results for $F_s^{(1)}(k, t)$ are plotted in figure 6 versus the *scaled time* $D_1 t$, for a wavenumber close to k_0, the position of the main peak in the static structure factor, and for five different values of the coupling Γ. The results for the three states in the supercooled liquid, above the glass transition, fall practically on a unique master curve. In the immediate vicinity of the glass transition ($\Gamma = 1.46$), the MD results for $F_s^{(\alpha)}(k, t)$ from different runs are less reproducible and the estimates of the diffusion constants D_α are more uncertain. Nevertheless we believe the deviations from the master curve observed beyond the glass transition ($\Gamma = 1.46$ and 1.48) to be significant, again in agreement with mode-coupling theory, which predicts a scaling regime for α-relaxation above the transition, but not below, since the system is then supposed never to attain a fully relaxed equilibrium state [12, 13].

5. Relaxation of the pair structure

The static pair structure of a binary mixture is described by the three partial distribution functions $g_{\alpha\beta}(r)$, and the gradual break-up of the initial structure is characterised by their time-dependent generalisations, i.e. the 'distinct' parts of the density autocorrelation (or Van Hove) functions, namely

$$G_d^{(\alpha\beta)}(r, t) = (1/N_\alpha N_\beta)^{1/2} \sum_{i=1}^{N_\alpha} {\sum_{j=1}^{N_\beta}}' \langle \delta(\boldsymbol{r} - \boldsymbol{r}_i^{(\alpha)}(0) + \boldsymbol{r}_j^{(\beta)}(t)) \rangle \tag{8}$$

where the prime means that the self-term $i = j$ is to be left out if $\alpha = \beta$. In the stable or slightly supercooled liquid, the initial structure decays rapidly and the $G_d^{(\alpha\beta)}(r, t)$ reach their uniform limit of unity after typically 10 Einstein periods $1/\Omega_E \sim \tau$. This 'structural relaxation' slows down dramatically, however, as the temperature is lowered towards the glass transition. An illustration of the phenomenon is provided by figures 7–9, which show one of the three $G_d^{(\alpha\beta)}(r, t)$ as a function of the reduced distance $x = r/\sigma_1$, for several values of the reduced time argument $t^* = t/\tau$, and for increasing values of the coupling Γ. At $\Gamma = 1.44$, figure 7, the relaxation is nearly complete after $t^* = 200$. The

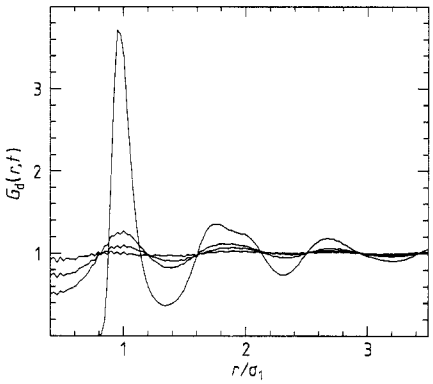

Figure 7. $G_d^{11}(r, t)$ plotted versus r/σ_1 at $\Gamma = 1.44$ and $t^* = 0$, 60, 120 and 240.

behaviour is qualitatively different at $\Gamma = 1.46$ (figures 8(*a*) and (*b*)). After an initial rapid decay, $G_d^{(\alpha\beta)}(r, t)$ appears to be practically stabilised over the time interval $20 \leqslant t^* \leqslant 100$. However, upon further increasing t^*, $G_d^{(\alpha\beta)}(r, t)$ resumes its decay, although this second stage of relaxation is much slower; even after $t^* = 480$, a considerable amount of structure remains. Evidently we are in the presence of a two-stage process. In the corresponding intermediate scattering function

$$F_d^{(\alpha\beta)}(k, t) = (1/N)\langle \rho_k^{(\alpha)}(t)\rho_{-k}^{(\beta)}(0)\rangle \tag{9}$$

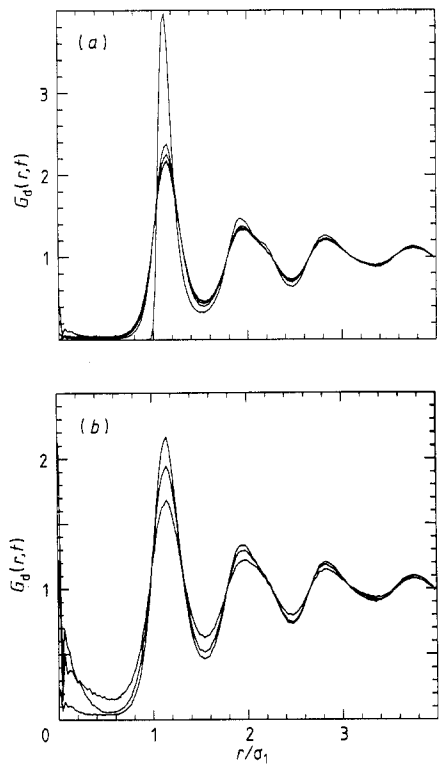

Figure 8. $G_d^{22}(r, t)$ plotted versus r/σ_1 at $\Gamma = 1.46$ and for $t^* = 0$, 18, 36, 54, 72 (*a*) and $t^* = 72$, 240, 480 (*b*).

calculated for a wavenumber k corresponding roughly to the period observed in r-space (i.e. to the position of the first peak in the static structure factor $S_{\alpha\beta}(k) = F_d^{(\alpha\beta)}(k, t = 0)$), the initial and final structural decay are separated by a nearly horizontal plateau. This is qualitatively similar to the behaviour observed for the self-parts of the density autocorrelation functions (cf. figure 6), and to the results of inelastic neutron scattering experiments [1]. For still stronger coupling ($\Gamma = 1.48$), the second relaxation stage is not observed any more, at least over the time interval covered by our MD simulations ($t^* \leq 500$); in other words, the initial structure $g_{\alpha\beta}(r)$ appears to decay towards a 'frozen' (time-independent) structure, rather than towards unity (figure 9). This is qualitatively similar to what is observed in the CsCl crystal phase of the same model, although the pair structure is very different in that case.

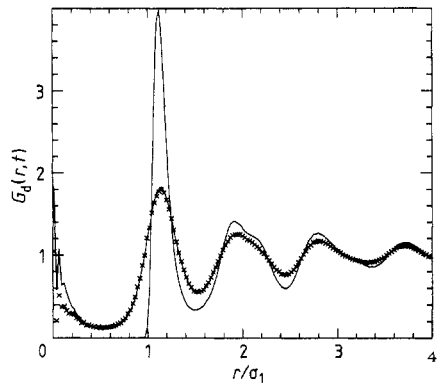

Figure 9. $G_d^{22}(r, t)$ plotted versus r/σ_2 at $\Gamma = 1.48$ for $t^* = 0$ and $t^* = 240$ (full curves) and $t^* = 480$ (crosses).

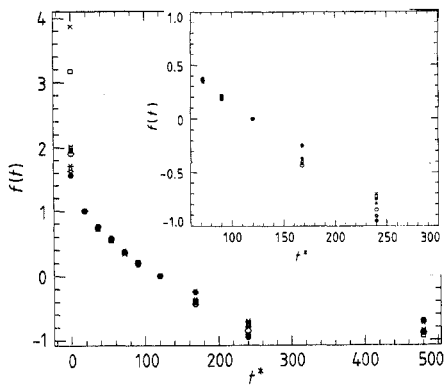

Figure 10. $f(t)$, as in formula (13), versus t^*, for $\Gamma = 1.46$ and $m_2/m_1 = 10$, taking $t_0^* = 18$ and $t_1^* = 120$. For each t^*, eight points are shown, corresponding to $n = 1$ to 8. Inserted is a detail of the same plot that shows the breakdown of the factorisation *ansatz* (10) for longer times.

As is clearly evident from all the cases shown in the figures, the amplitudes of the successive maxima and minima decrease with time, but their positions, as well as those of the nodes of $G_d^{(\alpha\beta)}(r, t) - 1$, do not change with time. This suggests a factorisation of the type predicted by mode-coupling theory in the β-relaxation regime [7]:

$$G_d(r, t) = G_d^{(0)}(r) + H(r)f(t) \tag{10}$$

where we have left out the species pair indices $\alpha\beta$. In order to test the *ansatz* (10), we have computed the 'scalar products'

$$a_n(t) = \int_{r_n}^{r_{n+1}} r^2[G_d(r, t) - 1][g(r) - 1]\,dr \tag{11}$$

where the r_n are the positions of successive nodes of $g_{\alpha\beta}(r) - 1$. These scalar products yield a measure of the rate at which the initial structure decays over a range of interatomic distances corresponding to successive shells of neighbours. Substitution of the *ansatz* (10) into (11) would yield for these scalar products the generic form

$$a_n(t) = \alpha_n + \beta_n f(t). \tag{12}$$

Below the ideal glass transition temperature, the α_n are a measure of the 'frozen' structure, while $f(t)$ describes the β-relaxation. If t_0 denotes some initial time characteristic of the short-time behaviour (Einstein regime) and t_1 a time corresponding roughly to the end of the β-relaxation regime, the relaxation function $f(t)$ is determined by the ratio

$$f(t) = \frac{a_n(t) - a_n(t_1)}{a_n(t_0) - a_n(t_1)} \tag{13}$$

where it is assumed that $f(t_1) = 0$. Results for the scalar products (11) at $\Gamma = 1.46$ and for the mass ratio $m_2/m_1 = 10$, plotted according to equation (13) as functions of t for several n, are shown in figure 10. The factorisation assumption is seen to be poor at very short times, but reasonable in the expected β-relaxation regime ($20 \leqslant t^* \leqslant 100$); at longer times the ratios (13) exhibit further decay, which may be associated with α-relaxation or residual activated processes. Overall, the factorisation *ansatz* (10) turns out to be a reasonable assumption only at intermediate times, which may correspond to β-relaxation.

6. Long-wavelength collective modes

Structural relaxation is most conveniently explored for wavelengths of the order of the inter-particle spacing, i.e. for wavenumbers $k \simeq k_0$, which correspond to maximum intensity of scattered radiation. At such short wavelengths, the density autocorrelation functions are dominated by single-particle motion, whereas collective modes are completely damped. At longer wavelengths ($k < k_0$), the density autocorrelation functions decay more and more slowly [15], since the characteristic relaxation time scales roughly like $(Dk^2)^{-1}$, but the influence of the longitudinal collective modes is expected to be superimposed on the slow structural relaxation. We have investigated the behaviour of longitudinal modes in the vicinity of the glass transition, by computing the mass density autocorrelation function

$$F^{(m)}(k, t) = (1/N)\langle \rho_k^{(m)}(t) \rho_{-k}^{(m)}(0) \rangle \tag{14}$$

where

$$\rho_k^{(m)}(t) = \sum_{i=1}^{N} (m_i/\mu) \exp(\mathrm{i}\boldsymbol{k} \cdot \boldsymbol{r}_i) \tag{15}$$

is the microscopic mass density, and $\mu = x_1 m_1 + x_2 m_2$ is the mean mass. In liquid mixtures, the hydrodynamic limit of $F^{(m)}(k, t)$ is governed by coupled inter-diffusion and heat diffusion modes and by the propagating sound mode [29]. The MD results for $F^{(m)}(k, t)$ at $\Gamma = 1.42$ are plotted versus time in figure 11, for the smallest wavenumber, k_1, compatible with the periodic boundary conditions, and for $k_2 = 2k_1$. It should be stressed that, while the mass structure factor $S^{(m)}(k) = F^m(k, t = 0)$ is subject to large statistical uncertainties for a given k, the difference $F^{(m)}(k, t) - F^{(m)}(k, t = 0)$ turns out to be much better defined and easily reproducible. The two curves displayed in figure 11 exhibit moderately damped oscillations with a slowly decaying envelope characteristic of well defined sound waves that propagate through a nearly frozen structure. The period and amplitude ratios of the oscillations determine the sound velocity and damping. Alternatively these may be determined from the position and width of the Brillouin peaks appearing in the mass fluctuation spectrum $S^{(m)}(k, \omega)$, which is the Fourier

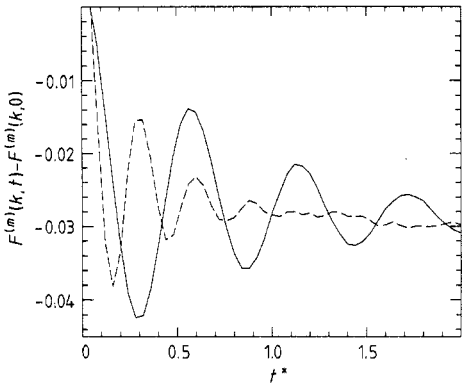

Figure 11. $F^{(m)}(k, t) - F^{(m)}(k, 0)$ versus t^* at $\Gamma = 1.42$, for $k = k_1$ (full curve) and $k = 2k_1$ (broken curve).

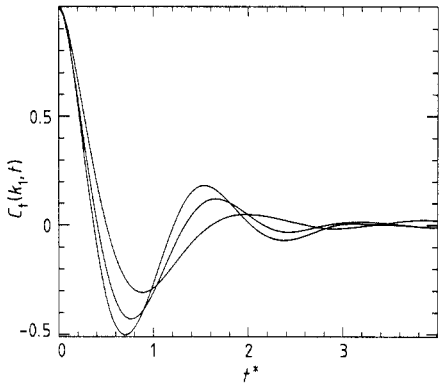

Figure 12. $C_t^{(m)}(k, t)$ versus t^* for $k = k_1$, and for, from right to left, $\Gamma = 1.3$, 1.38 and 1.455. The latter result has in fact been obtained for a mass ratio $m_2/m_1 = 10$, but the corresponding time axis has been rescaled by the square root of the ratio of the total masses, $\sqrt{(3/11)}$.

transform of $F^{(m)}(k, t)$. There is some ambiguity in determining $S^{(m)}(k, \omega)$ from the MD data for $F^{(m)}(k, t)$, because of the very slow decay of the latter, which leads to a very sharp quasi-elastic peak in the frequency spectrum. Sound velocities and damping constants determined for several couplings Γ are listed in table 3. In the supercooled fluid ($\Gamma < \Gamma_0$), the sound velocity c_s is determined by the adiabatic bulk modulus

$$B_s = \rho(\partial P/\partial\rho)_s = \rho\gamma(\partial P/\partial\rho)_T$$

(where $\gamma = C_p/C_v$ is the specific heat ratio), according to

$$c_s = (B_s/\rho\mu)^{1/2}.$$

The *isothermal* sound velocities c_T, which differ from c_s by a factor γ, have been calculated directly from the isothermal compressibilities and are also listed in table 3.

Table 3. Sound velocity c and sound absorption coefficient λ: λ is estimated as the width at half-height of the sound peak of $S^{(m)}(k_1, \omega)$; c_1 and c_2 (in units of σ_1/τ) are respectively the sound velocity deduced from the position of the peak and the isothermal velocity calculated from the measured elastic constants.

Γ	$\lambda\tau$	c_1	c_2
1.0	2.9	6.3	5.66
1.2	2.8	8.6	7.46
1.3	3.8	9.8	8.47
1.35	3.4	10.7	8.91
1.38	3.8	10.6	9.31
1.41	3.3	11.1	9.70
1.43	3.2	11.9	9.93
1.45	3.5	12.1	10.26
1.48	3.6	12.3	10.68
1.50	3.5	12.6	11.04

Since γ is estimated to fall in the range 1–1.1 for the states considered here, the values for c_T and c_s, respectively determined from the equation of state and from the position of the Brillouin peak, are clearly compatible. In the glass ($\Gamma > \Gamma_0$), the sound velocity is related to the adiabatic bulk and shear moduli B_s and G_s by

$$c_s = [(B_s + 4G_s/3)/\rho\mu]^{1/2}.$$

Near the transition, G_s is small compared to B_s [19] so that c_s is essentially determined by B_s as in the supercooled liquid.

The most important conclusion to be drawn from inspection of table 3 is that the sound attenuation (defined as the imaginary part of the complex sound frequency) is practically constant over the range of coupling constants investigated ($1 \leqslant \Gamma \leqslant 1.5$), for the smallest wavenumber k_1; since the sample was gradually compressed to increase Γ, the reduced wavenumber $k_1\sigma_1$ increases slightly (according to the one-third power of Γ). In the stable fluid phase, sound attenuation is determined by viscosity, thermal conductivity and inter-diffusion [30], the viscous damping mechanism being generally the most efficient. The standard expression for the sound attenuation coefficient, derived from the linearised Navier–Stokes equations, would predict a dramatic increase of sound damping with decreasing temperature, since the viscosity increases sharply as the glass transition is approached. However the predictions of hydrodynamics are valid only for frequencies ω less than the characteristic frequency $\omega_0 = c_s^2/(4\nu/3 + \nu')$, where ν and ν' denote the kinematic shear and bulk viscosities [29]. The value of ω_0 may be estimated from the viscosities calculated by Heyes [31] for a one-component soft-sphere fluid, via the conformal solution *ansatz* (3). Above the freezing temperature ($\Gamma \leqslant 1.2$), ω_0 is significantly larger than the acoustic frequency $\omega_1 = c_s k_1$ corresponding to the smallest wavenumber k_1, so that the hydrodynamic expression for the sound attenuation coefficient should be applicable. However, as the viscosity increases rapidly in the supercooled liquid, on approaching the glass transition, the hydrodynamic frequency range shrinks to zero, so that the condition $\omega_1 = c_s k_1 \ll \omega_0$ is no longer satisfied. For frequencies $\omega > \omega_0$ the medium behaves elastically, and sound attenuation is dominated by anharmonic effects similar to the damping mechanisms in crystalline solids. The important observation made here is that the cross-over from viscous (fluid-like) damping to anharmonic (solid-like) damping of sound waves at a given wavelength occurs very smoothly, since it is characterised by a nearly constant value of the sound absorption coefficient. A detailed theoretical analysis of the damping of sound in the vicinity of the glass transition, incorporating the effects of slow structural relaxation, remains to be done.

We have also computed the transverse mass current autocorrelation function

$$C_t^{(m)}(k, t) = (1/Nk^2)\langle[\boldsymbol{k} \times \boldsymbol{j}_{\boldsymbol{k}}^{(m)}(t)] \cdot [\boldsymbol{k} \times \boldsymbol{j}_{-\boldsymbol{k}}^{(m)}(0)]\rangle \tag{16}$$

where $\boldsymbol{j}_{\boldsymbol{k}}^{(m)}(t)$ is the microscopic mass current

$$\boldsymbol{j}_{\boldsymbol{k}}^{(m)}(t) = \sum_{i=1}^{N} m_i \boldsymbol{v}_i(t) \exp[\mathrm{i}\boldsymbol{k} \cdot \boldsymbol{r}_i(t)]. \tag{17}$$

Examples of $C_t^{(m)}(k, t)$, computed for the smallest wavenumber $k = k_1$, are shown in figure 12. The correlation function exhibits oscillations, characteristic of a propagating shear mode, which are more and more pronounced as the coupling increases. This viscoelastic behaviour is observed only for significantly shorter wavelengths, of the order of the inter-atomic spacing, in the stable liquid phase [30]. This qualitative difference

between the behaviour in the stable and supercooled liquid phases agrees with a simple viscoelastic analysis, which predicts that shear waves will appear for wavenumbers k larger than a critical wavenumber $k_c \sim 1/\eta$ [30]. In the vicinity of the glass transition k_c becomes much smaller than the minimum wavenumber k_1 compatible with the size of the simulation cell, thus allowing the propagation of a well defined shear mode similar to transverse phonons in solids. The frequency of the observed shear mode turns out to be less than half the frequency of the longitudinal sound mode at the same wavelength.

7. Conclusions

In order to characterise the structural slowing down in the vicinity of the glass transition of a simple binary alloy, we have examined the relaxation of the coherent and incoherent parts of the density autocorrelation functions both in r- and in k-space. We have found that the statistical uncertainties are considerably smaller for the r-space Van Hove functions than for the k-space intermediate scattering functions, a situation familiar from molecular dynamics or Monte Carlo simulations of the static equivalents, i.e. the pair distribution functions and the structure factors. This reduction of the statistical uncertainties combined with improved reproducibility of the computed correlation functions, due to very careful quenches of the samples, allows us to formulate well defined diagnostics of a sharp glass transition.

The first diagnostic concerns the self Van Hove functions $G_s^{(\alpha)}(r, t)$. The peak in $r^2 G_s^{(\alpha)}(r, t)$ decays differently above and below the transition temperature. For $\Gamma < \Gamma_0$ ($\simeq 1.46$ in the case under investigation), the peak broadens and moves to larger r with increasing time; while for $\Gamma > \Gamma_0$, the peak position is frozen, i.e. the peak decays without moving to longer times. The self-diffusion constants do not go strictly to zero, however, and activated 'hopping' processes give rise to a 'tail' in $G_s^{(\alpha)}$ at larger distances.

The second diagnostic is related to the distinct Van Hove functions $G_d^{(\alpha\beta)}(r, t)$. While for $\Gamma < \Gamma_0$, these correlation functions decay rather rapidly and continuously to their asymptotic value of unity, their relaxation becomes a much slower two-step process above Γ_0: after an initial decay (which may be identified with β-relaxation), the functions are practically constant over a time interval that expands as Γ increases. Only in the immediate vicinity of the glass transition is it possible to observe the subsequent α-relaxation within the duration of the present MD simulations. It is interesting to note that during the initial relaxation of the $G_d^{(\alpha\beta)}(r, t)$, the amplitudes of only the first two peaks decay with time, whereas the subsequent peaks appear to be unaffected, in qualitative agreement with a recent mode-coupling calculation for the glass transition of the hard-sphere system [32].

Both diagnostics lead to the same estimate of the glass transition parameter Γ_0. A series of runs carried out for the mass ratio $m_2/m_1 = 10$ show a behaviour very similar to that observed for $m_2/m_1 = 2$, and lead to a practically identical estimate of Γ_0 ($\Gamma_0 = 1.47$ instead of 1.46). Note, however, that equilibration in the vicinity of the glass transition appears to be significantly slower for the system with the larger mass ratio.

Overall the results of the present simulations are compatible with the glass transition scenario suggested by the more elaborate versions of mode-coupling theory, but the statistical uncertainties prevent a fully quantitative test of the various scaling regimes predicted by this theory.

Acknowledgments

The authors wish to thank Bernard Bernu for useful suggestions. JNR gratefully acknowledges the financial support of the Corps des Ponts et Chaussées.

References

[1] Mezei F, Knaak W and Farago B 1987 *Phys. Rev. Lett.* **58** 571; 1987 *Phys. Scr.* **T19** 363
[2] Knaak W, Mezei F and Farago B 1988 *Europhys. Lett.* **7** 529
[3] Fujara F and Petry W 1987 *Europhys. Lett.* **4** 921
[4] Frick B, Richter D, Petry W amd Buchenau U 1988 *Z. Phys.* B **70** 73
[5] Leutheusser E 1984 *Phys. Rev.* A **29** 2765
[6] Bengtzelius U, Götze W and Sjölander A 1984 *J. Phys. C: Solid State Phys.* **17** 5915
[7] Götze W 1985 *Z. Phys.* B **60** 195
[8] De Raedt H and Götze W 1986 *J. Phys. C: Solid State Phys.* **19** 2607
[9] Bengtzelius U 1986 *Phys. Rev.* A **33** 3433
[10] Bosse J and Thakur J S 1987 *Phys. Rev. Lett.* **59** 998
[11] Götze W and Sjögren L 1987 *J. Phys. C: Solid State Phys.* **20** 879
[12] Götze W and Sjögren L 1987 *Z. Phys.* B **65** 415; 1988 *J. Phys. C: Solid State Phys.* **21** 3407
[13] Das S P and Mazenko G F 1986 *Phys. Rev.* A **34** 2265; 1987 *Phys. Rev.* A **36** 211
[14] Ullo J J and Yip S 1985 *Phys. Rev. Lett.* **54** 1509
[15] Pastore G, Bernu B, Hansen J P and Hiwatari Y 1988 *Phys. Rev.* A **38** 454
[16] Miyagawa H, Hiwatari Y, Bernu B and Hansen J P 1988 *J. Chem. Phys.* **88** 3879
[17] Bernu B, Hansen J-P, Hiwatari Y and Pastore G 1987 *Phys. Rev.* A **36** 4891
[18] Mountain R D and Thirumalai D 1987 *Phys. Rev.* A **36** 3300
[19] Barrat J L, Roux J N, Hansen J-P and Klein M L 1988 *Europhys. Lett.* **7** 707
[20] Nosé S and Yonezawa F 1985 *Solid State Commun.* **56** 1005
[21] Barrat J L, Baus M and Hansen J-P 1987 *J. Phys. C: Solid State Phys.* **20** 1413
[22] Jonsson H and Andersen H C 1988 *Phys. Rev. Lett.* **60** 2295
[23] Hiwatari Y 1979 *J. Phys. Soc. Japan* **47** 733; Kambayaski S and Hiwatari Y 1987 *J. Phys. Soc. Japan* **56** 2788
[24] Hansen J-P 1970 *Phys. Rev.* A **2** 221
[25] Hoover W G, Ross M, Johnson K W, Henderson D, Barker J A and Brown B C 1970 *J. Chem. Phys.* **52** 4931
[26] Verlet L 1967 *Phys. Rev.* **159** 98
[27] Rogers F J and Young D A 1984 *Phys. Rev.* A **30** 999
[28] Edwards S F and Anderson P W 1975 *F. Phys. F: Met. Phys.* **5** 965
[29] Bhatia A B 1967 *Ultrasonic Absorption* (Oxford: OUP)
[30] Hansen J P and McDonald I R 1986 *Theory of Simple Liquids*, 2nd edn (London: Academic)
[31] Heyes D M 1983 *J. Chem. Soc., Faraday Trans.* II **79** 1741
[32] Barrat J L, Götze W and Latz A 1989 *J. Phys.: Condens. Matter* **1** 7163–70